EFFECT OF SILICON SUBSTITUTION ON THE ZIGZAG SINGLE-WALLED CARBON NANOTUBES WITH VARIOUS DIAMETERS

N.N. YUAN [a, b], H.C. BAI [a*], Y.J. MA [a, b], Y.Q. JI [a, b]
[a]*Key Laboratory of Energy Sources and Chemical Engineering, State Key Laboratory Cultivation Base of Natural Gas Conversion, Ningxia University, Yinchuan, Ningxia 750021, China*
[b]*School of Chemistry Science and Engineering, Ningxia University, Yinchuan, Ningxia 750021, China*

The effect of silicon substitution on the structures, relative stabilities and properties of zigzag carbon nanotubes (CNTs) have been studied by using the first-principle calculations is this work. The quantitative descriptions from viewpoint of the pi-orbital axis vector theory, relative stability, defect formation energy, electronic structure and aromaticity of the doped tubes has been addressed and compared with the pure ones systemically and in details. The pyramidalization angles of the silicon are much larger than those of carbon according to the pi-orbital axis vector analysis. The computed defect formation energies suggest that the Si-doping would be contained easier in small CNTs. A quantitative relation between the defect formation energy and the curvature of the Si-doped tubes is obtained. The frontier molecular orbitals exhibit obvious localization at the edge regions for both doped and un-doped tubes. Moreover, the doping effect on the aromaticity is also studied based on the probe of nuclear independent chemical shift.

1. Introduction

Due to the state-of-the-art potentials in physics, chemistry, material science and nanotechnology, carbon nanotubes (CNTs), especially the single-walled carbon nanotubes (SWCNTs) have attracted great deal of attention. It is known that the physical property of a SWCNT mainly depend on the diameter as well as chirality. Especially, the electronic properties of CNTs could be modified by various physical or chemical methods, such as electronic field [1], vacant defect [2], encapsulation [3–4], and physical or chemical adsorptions on the side wall of the tubes [5–6].

On the other hand, the doped CNTs can be obtained if one or more carbon atoms of the tubes are substituted by heteroatoms. These hybrid CNTs recently have become good candidates with unique structural, electronic and elastic properties, which are much different from those of the pristine ones due to the existence of heteroatoms [7-8]. Therefore, doping of substitution is also one of the important strategies to modulate properties of CNTs. Most recently, Si-doped SWCNTs have been synthesized using chemical vapor deposition method for the first time [9]. This new species of doped CNTs should be interesting nano-scaled materials to be expected in the future.

As for the theoretical side, several literatures have pad attentions to the hybrid CNTs containing heteroatoms [10–23]. However, most investigations focus on N- or B- doped CNTs. Previous computations on Si-doped CNTs are limited on one or two selected SWCNTs

---

*Corresponding author: hongcunbai@foxmail.com

substitutionally doped by silicon atoms. For instance, the zigzag (10, 0), (8, 0) and (5, 5) tubes doped by silicon atoms were calculated by Fagan, Bian and Jiang as well as their co-workers and Zardoost et. al., pay attention to Si-doped doped (6, 3) tube [18–23]. Thus further investigation is still necessary to get more understanding about the Si-doped CNTs. Additionally, only a few theoretical studies are available on this issue according to our best knowledge, and the following topics still need to be addressed: (a) the quantitative description of silicon doping on CNTs deformation from viewpoint of the pi-orbital axis vector (POAV) theory; (b) the roles of silicon doping on molecular orbital, electronic structure and functional property of CNTs; (c) the diameter-dependent or -independent effects on structures, relative stabilities and properties of Si-doped CNTs.

In this paper, we carried out theoretical studies on silicon substitutionally doped armchair SWCNTs with various diameters by means of self-consistent field molecular orbital (SCF–MO) method under the framework of density functional theory (DFT). The structure, stability, electronic property hyperpolarizability and aromaticity of the hybrid CNTs are calculated and compared with those of pure ones. We hope the studies would be helpful for promotion of this state-of-the-art research subject.
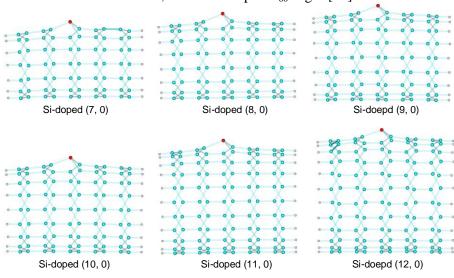
2. Models and Computational Methods

Usually a SWCNT can be denoted with a pair of integers (n, m), and classified into three types, namely, armchair nanotubes (n, n), zigzag nanotubes $(m, 0)$, and chiral nanotubes (n, m) with $n \neq m$. We limit to zigzag CNTs in this paper. In order to investigate the size-effect induced by various tube diameters, the pure and Si-doped armchair SWCNT $(m, 0)$ with m=7–18 were considered. These tubes have diameters in the range of 5–14 Å, which covers the usual SWCNTs obtained in experiments [24, 25]. The armchair SWCNTs with finite lengths of 2.5 unite cells are selected to study the silicon doping effect. These finite CNTs have the lengths of about 1.0 nanometer. Actually, the (12, 0) tubes with lengths up to 5 unite cells are also calculated, and the main conclusions are not changed according to our previous studies [14]. The dangling bond for the carbon atoms at the edges is terminated by a hydrogen atom in the models to keep all the carbon atoms are three-coordinated, and this is a common treatment of finite CNTs [14, 26]. Thus it contains $10 \times m$ carbon atoms and $2 \times m$ hydrogen atoms for the model of pristine tube $(m, 0)$. The initial structures of the Si-doped tubes are obtained by replacing the middle carbon atom in CNT by a silicon atom.

The hybrid functional method B3LYP within the scope of DFT is adopted to calculate the doped CNTs. The geometrical optimization, energy and electronic property are all computed using the Kohn-Sham SCF-MO method at B3LYP/6-31G* level with Gaussian 09 program [27]. According to the previous calculations, the B3LYP method has been successfully applied to the theoretical studies on carbon-based materials obtained by doping the CNTs and fullerenes [13–15, 18, 28], and the methods used here could give rather good results compared with those obtained by various different functional and basis sets [29].

3. Results and discussion
3.1 Geometrical Structure

Several structures of Si-doped $(m, 0)$ n=7–18 tubes with full geometrical optimization are shown in Fig. 1. It is clearly that the structural rearrangement and vacant defect are not occurred to these Si-doped tubes, and they still exhibit tubal form. It is similar to the B- and N- doped CNTs [10, 11, 15]. However, compared with B- and N- doped CNTs, the geometrical distortion in the Si-doped CNTs is more obvious. It is evident that the silicon atoms tend to "pop out" from the original positions for all the Si-doped tubes, as shown in Fig. 1. It comes without surprise since carbon atom is much smaller than silicon, whereas it is close to boron and nitrogen atoms. The

similar case could also be found in B-, N- and Si-doped C_{60} cages [28].

Fig. 1 The optimized structures of Si-doped zigzag CNTs

In order to evaluate the distortion of the doped tubes quantitatively, the pi-orbital axis vector (POAV) analysis [30] is performed for the carbon and heteroatoms. According to the POAV theory, the pyramidalization angle θ_P is defined as:

$$\theta_P = (\theta_{\sigma\pi} - 90)° = (180 - \theta - 90)° = (90 - \theta)° \tag{1}$$

Here we use the solution method we developed to perform the POAV analysis [31]. The angle θ can be obtained by

$$\theta = \arccos(\frac{\left| l(x_a - x_o) + m(y_a - y_o) + n(z_a - z_o) \right|}{\sqrt{(x_a - x_o)^2 + (y_a - y_o)^2 + (z_a - z_o)^2}}) \tag{2}$$

where l, m and n can be obtained by O (x_o, y_o, z_o), A (x_a, y_a, z_a), B (x_b, y_b, z_b) and C (x_c, y_c, z_c), which are the coordinates of the conjugated atom (O) and its three attached atoms (A, B and C), respectively. The detailed descriptions can be seen from our previous studies [31]. As listed in Table 1, the POAV angles are about 2.9–7.4 ° for the carbon atoms in pure CNTs, which are all smaller than 11.6° in fullerene C_{60}. It gives smaller POAV angles in larger tubes due to the less strain in the tubes with large diameters. As to POAV of silicon atoms in the doped tubes, they are in the range of 22.5–27.9 °. The POAV angles of silicon atoms decrease as the tubes become larger. It is very clearly that the obtained POAV angles of the silicon in the doped tubes are much larger than those of carbon atoms. This is due to the fact that the silicon is more favorable to sp^3 hybridization. The evidence can be found in large tubes. For example, the POAV angle of silicon atom is gradually reduced to 22.5 ° in (18, 0) doped tube, which is close to 20.1° obtained in Si-doped graphene. This value is only slightly larger than 19.5 ° for standard sp^3 hybridization.

Now we focus on the bond lengths in the doped CNTs. Two types of bond are present in the zigzag SWCNTs, the ones parallel to tube axis b_1 and the others with some angles to tube axis b_2. As one carbon atom is repealed by silicon, the Si—C bonds are presented. The obtained C—Si bond lengths (1.764–1.849 Å as shown in Table 1) are much larger than those of the C—C bond lengths. Furthermore, the C—C bond lengths near the silicon atom change more obvious. As in the region away from the Si atom, the bond lengths are almost unchanged.

Table 1. The obtained bond length of C—Si (b_1 and b_2), pi-orbital axis vector angle of carbon or silicon (POAV), energy gap (E_g) and the amount of charge transfer (CT) of the tubes. (b_1 and b_2 in Å; POAV in degree; E_g in eV and CT in electron).

Tube	POAV	E_g	Si-doped tube	b_1	b_2	POAV	E_g	CT
(7, 0)	7.4	0.343	(7, 0)	1.785	1.849	27.9	0.363	0.287
(8, 0)	6.5	0.285	(8, 0)	1.796	1.836	28.0	0.282	0.242
(9, 0)	5.8	0.298	(9, 0)	1.777	1.810	25.4	0.305	0.270
(10, 0)	5.4	0.198	(10, 0)	1.766	1.788	23.0	0.177	0.237
(11, 0)	4.7	0.260	(11, 0)	1.771	1.794	24.1	0.263	0.252
(12, 0)	4.4	0.310	(12, 0)	1.761	1.782	22.8	0.328	0.268
(13, 0)	4.0	0.267	(13, 0)	1.768	1.785	23.4	0.257	0.244
(14, 0)	3.7	0.278	(14, 0)	1.767	1.783	23.1	0.279	0.241
(15, 0)	3.4	0.260	(15, 0)	1.767	1.780	23.0	0.253	0.237
(16, 0)	3.3	0.239	(16, 0)	1.764	1.777	22.6	0.235	0.225
(17, 0)	3.3	0.252	(17, 0)	1.765	1.776	22.6	0.247	0.249
(18, 0)	2.9	0.214	(18, 0)	1.765	1.774	22.5	0.213	0.221

3.2 Energy and Relative Stability

In order to study the thermodynamic stability of the Si-doped CNTs, the cohesive energy (E_{coh}) per atom is calculated by equation:

$$E_{coh} = (E_{tube} - N_c E_c - N_{Si} E_{Si} - N_H E_H)/(N_C + N_{Si} + N_H) \tag{3}$$

where E_{tube} and E_i (i=C, Si and H) are the energies of the tubes and isolated C, Si and H atoms, while N_i is the number of C, Si and H atoms. Here the system with larger E_{coh} is more stable. The obtained results are listed in Fig. 2(a). We can see that E_{coh} of the pure tubes with various diameters are calculated to be 6.261–6.475 eV/atom. It is evident that the CNTs with large diameters are energetically more stable due to less strain. As for the Si-doped tubes, E_{coh} are in the range of 6.199–6.445 eV/atom, and slightly smaller than that of the corresponding pristine as detected from Fig. 2(a). Thus the introduced Si atom would decrease the thermodynamic stability of the tubes from viewpoint of cohesive energy. However, the E_{coh} of large doped tubes are still larger than those of the small ones.
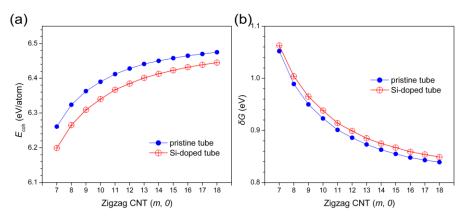
Fig. 2 The calculated energies of the tubes. (a): cohesive energy, E_{coh} and (b): Gibbs free energy, δG.

As the doped CNTs studied here have different chemical compositions, we also adopt the Gibbs free energy, δG, to analyze the relative stability of the doped CNTs. It should be pointed out that this approach is customarily used to account for the relative stabilities with various chemical compositions [32,33]. Here in this paper δG is defined through the equation:

$$\Delta G = -E_{\text{coh}} + x_C\mu_C + x_{Si}\mu_{Si} + x_H\mu_H \tag{4}$$

where E_{coh} is the cohesive energy of the systems as mentioned above, x_i is the molar fraction for different atoms, and μ_i is the chemical potential of the constituents at a given state. We choose μ_H, μ_C and μ_{Si} as the binding energy per atom of the H_2 molecule, graphene and silicone, and the values are calculated to be 2.380, 8.300 and 4.050 eV, respectively. This definition allows for a direct energy comparison of the doped CNTs with different chemical compositions. The system with smaller δG is more stable. The obtained values of δG for the tubes studied are listed in Fig. 2(b).
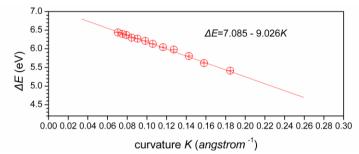
As can be seen from the figure, the calculated δG of the pure tubes with different diameters is in the range of 0.839–1.052eV. Thus a CNT with large diameter is energetically more stable from viewpoint of Gibbs free energy, and this is consistent with the result of cohesive energy. As the silicon doping, the values of δG are ranged from 0.849 to 1.063 eV for the doped series, and somewhat larger than that of the corresponding pristine tube. Thus, the same as the conclusion drawn from the cohesive energies, the introduced Si atom would decrease the relative stability of the tubes also from viewpoint of the Gibbs free energies.

The defect formation energy (ΔE) of the doped tubes is also considered, and it can be calculated by:

$$\Delta E = E_{\text{doped-tube}} + E_C - E_{\text{CNTs}} - E_{Si} \tag{5}$$

where $E_{\text{doped-tube}}$ and E_{CNTs} respectively are the energies of the doped and pure tubes with the minimum structure. From Fig. 3, we can see that ΔE of the doped CNTs are all positive, indicating that the formations of the Si-doping defect are all endoergic. Thus it is not energetically favorable to form the Si-doped CNTs from viewpoint of total energy change. The obtained ΔE values are in the range of 5.174–6.436 eV for the doped tubes studied here. It is observed that thin tubes exhibit small values of ΔE, indicating that the Si-doped defects more likely occur to CNTs with small diameter. As a comparison, ΔE of Si-doped graphene with finite sizes is also calculated. The obtained result is 6.983 eV, and always larger than those of the CNTs here. ΔE for the formation of $C_{59}Si$ from fullerene C_{60} cage is also calculated to be 4.961 eV, and which are all smaller than those for the Si-doped tubes here. Thus it seems that formation energies of Si-doped structures have something to do with the curvature: the carbon-based nanostructures with large curvature

exhibit small ΔE. Recall that the POAV angles of the CNTs are in the range of 2.9–7.4 °, which are smaller than 11.6 ° in C$_{60}$, but larger than zero degree in graphene as mentioned above.

Fig. 3 The relationship of the defect formation energies (ΔE) and curvature K of the Si-doped tubes.

In order to get quantitative information about the curvature-dependent formation energies of Si-doped defects, in Fig. 3 we also plot ΔE respect to curvature K, which is treated as the inverse of the CNTs diameter. It is very interesting that the defect formation energy is linear-scale with the tube curvature based on the equation $\Delta E=7.085–9.026K$ with correlation coefficient R>0.99 for these Si-doped armchair SWCNTs. The value of ΔE at zero curvature gives 7.085 eV according to the equation, which agrees with the obtained 6.983 eV for Si-doped graphene.

3.3 Electronic Property

Since the highest occupied molecular orbital (HOMO) and the lowest unoccupied molecular orbital (LUMO) play an important role in chemical reactions for the reactant, the energy levels of the frontier molecular orbital (FMO) for the series of tubes are listed in Fig. 4. It can be observed that HOMO and LUMO energy levels of all the Si-doped CNTs vary very little (less than 0.051 eV) compared with those of the pristine tubes. Although Koopmans' theorem is not fully valid for DFT calculations, the relative positions of the computed HOMO and LUMO reflect their abilities to lose and gain electrons, and this will be internally consistent within a series of tubes with various diameters. Thus the abilities to lose and gain electrons change very little when the Si atom is introduced into CNTs.
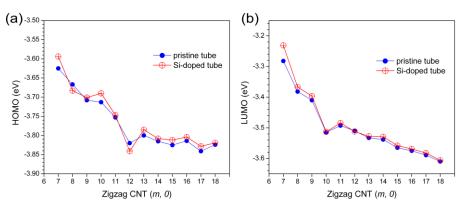

Fig. 4 The calculated electronic properties of the tubes. (a): HOMO and (b): LUMO.

The calculated HOMO-LUMO energy gaps (E_g) of the Si-doped CNTs are listed in Table 1. The obtained E_g of doped tubes are very similar to those of the pure ones, and the difference is within 0.021 eV. This result comes without much surprise since the HOMO and LUMO changed only a bit upon the silicon doping as mentioned above.

It should be pointed out that silicon shares the same column of the Periodic Table with carbon, and doping CNTs with silicon does not alter the valence electrons, which is different from N- and B- substitutions. Thus the electronic structure of the Si-doped CNTs would likely to be similar to that of pristine CNTs from viewpoint of total occupancy of the energy levels. This is confirmed by the distributions of HOMO and LUMO of the tubes. As shown in Fig. 5, the FMO of the pure tubes present obvious localization at the edge regions. This fact agrees with the former DFT calculations [34]. As the silicon is introduced, the localization feature at the edge regions is mainly retained for the FMO of Si-doped tubes. It is clearly that nearly no distribution is presented at the silicon site, except for LUMO of Si-doped (7, 0). This explains why the HOMO, LUMO and E_g of the zigzag tubes changes very little upon the silicon doping.
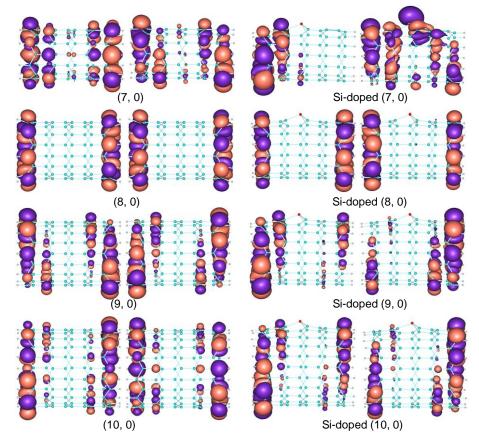

Fig. 5 The HOMO (left) and the LUMO (right) of pristine and Si-doped tubes. The FMO of (11, 0)–(18, 0) are similar to those of (10, 0) and not shown here.

Now we turn to the charge distribution of the doped tubes. Since silicon is less electronegative than carbon, the electronic charge transfer from Si atom to the neighbouring carbon atoms is occurred for these Si-doped tubes. It is found that the amount of charger transfer is in the range of 0.221–0.287 e according to the Mulliken population analysis as listed in Table 1. These values of charger transfer are less than 0.344 e for that of silicon doped C_{60}. We are also

aware that silicon atom exhibits more electrons in the larger tubes than in those smaller ones. As in Si-doped (18, 0) tube, the amount of charger transfer is reduced to 0.221 *e*, which close to 0.212 *e* for silicon doped graphene.

3.4 Aromaticity and Nuclear Independent Chemical Shift

The concept of aromaticity is significant in chemistry and could be explained by the ring current theory. In this study we evaluated the aromaticity by using the nuclear independent chemical shift (NICS), which has proven to be a simple and efficient probe [35–38]. To obtain the NICS indices, Bq ghost atoms are placed in the selected positions, and the chemical shifts of nuclear magnetic resonance are calculated at B3LYP/6-31G* level with the gauge independent atomic orbital (GIAO) approach. Then NICS is treated as the negative of the isotropic magnetic shielding constant of the ghost atom. The negative NICS value indicates the aromaticity, whereas the positive signifies anti-aromaticity [35].
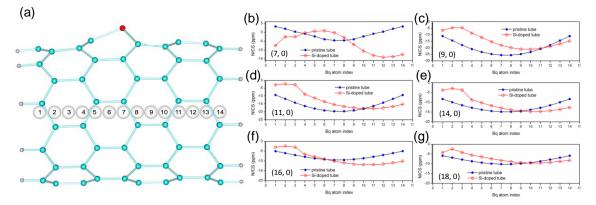

Fig. 6 The Bq atom index (a) and the computed NICS scan along the tube axis (b)–(g).

In this study we focus on the aromaticity inside tubes and thus 14 ghost atoms are placed at the ring central along the tube axis as shown in Fig. 6(a). By doing the NICS scan, a vivid picture of aromaticity along the tube axis could be achieved. The curves of computed NICS of pure and Si-doped (7, 0), (11, 0), (16, 0) and (18, 0) tubes are polluted as shown in Fig. 6. It is observed that the NICS distributions display nearly parabola shape for all the pure tubes, which is also confirmed by previous DFT calculations [39, 40]. This is due to the existence of a symmetric center of the zigzag models in our studies. As silicon is cooperated, the symmetric center is disappeared and thus the parabola curve of the NICS is also vanished. We are aware that Si-doped (7, 0) tube exhibit distinct aromatic behaviors compared with those larger ones. This can be ascribed to the large σ- and π-orbital rehybridization due to the very small diameter according to previous studies [41]. As to the larger tubes, the negative values of NICS suggest the aromatic properties along the tube axis. As shown in Figure 5, the obtained NICS of the doped tubes are less negative than those of pure ones at the left part of tube axis, indicating the decreased aromaticity upon the silicon substitution. However, in the right part, things are just opposite, and the aromaticity is enhanced as the silicon impure is present. As the tube become larger, the differences of NICS between the pure and doped tubes are more and more minor. For instance, the maximum difference of NICS at the tube axis is only 4.4 ppm for the pure and doped (18, 0) tube, while the values are 15.7 and 11.4 ppm for (7, 0) and (11, 0) tube, respectively. This is because the magnetic and electronic response at the tube axis upon the Si-doping would be weaker and weaker as the tubes become larger.

It has been pointed that NICS at the center of nano-clusters have essentially the same values as the endohedral helium chemical shifts [42], these obtained values are also helpful for the possible characterization of these doped tubes.

4. Conclusion

In summary, theoretical studies on Si-doped zigzag CNTs with various diameters have been performed using the SCF-MO method based on DFT calculations. The structures, relative stabilities, electronic and aromatic properties of the hybrid CNTs are calculated and compared with those of the pure ones. It is found that the obtained POAV angles of the silicon in the doped tubes are in the range of 22.5–27.9 °, and much larger than those of carbon atoms, due to the strong tendency of sp^3 hybridization. According to the results of cohesive energy and Gibbs free energy, the stability of the tubes would be decreased upon the silicon doping. Thin tubes exhibit small values of defect formation energy, and thus the Si-doping occurs easier in thin CNTs. Also we obtained the quantitative relation about the curvature-dependent formation energy with the equation $\Delta E=7.085–9.026K$. The obtained HOMO, LUMO and E_g of the zigzag tubes changes very little upon the silicon doping since the localization feature at the edge regions is mainly retained for the FMO of Si-doped tubes. The results of NICS scan suggest the aromatic property along the tube axis for both pure and doped tubes.

References

[1] A. Oliva-Avilés, F. Avilés, V. Sosa, A. Oliva, F. Gamboa, Nanotechnology
    23, 465710 (2012).
[2] T. Nongnual and J. Limtrakul, J. Phys. Chem. C **115**, 4649 (2011).
[3] W. Qiao, H. Bai, Y. Zhu, Y. Huang, J. Phys.: Condens. Matter **24**, 185302 (2012).
[4] W. Qiao, X. Li, H. Bai, Y. Zhu, Y. Huang, J. Solid State Chem. **186**, 64 (2012).
[5] B. Soleimani, S. Rostamnia, A. Ahmadi, Dig. J. Nanomater. Biostruct. **5**, 153 (2010).
[6] A. Li, L. Wang, M. Li, Z. Xu, P. Li, Z.Z. Zhang, Dig. J. Nanomater. Biostruct. **9**, 599 (2014).
[7] D. J. Li, U. N. Maiti, J. Lim, D. S. Choi, W. J. Lee, Y. Oh, G. Y. Lee, S. O. Kim,
    Nano Lett. **14**, 1228 (2014).
[8] R. Geetha, V. Gayathri, Superlattice Microstruct. **48**, 41 (2010).
[9] J. Campos-Delgado, I. O. Maciel, D. A. Cullen, D. J. Smith, A. Jorio, M. A. Pimenta,
    H. Terrones, M. Terrones, ACS Nano **4**, 1696 (2010).
[10] C. Yeung, Y. Chen, Y. Wang, J. Nanotechnol. **2010**, 801789 (2010).
[11] M. Naraghi, Carbon Nanotubes - Growth and Applications, Chapter 5, InTech Press, (2011).
[12] C. Tabtimsai, V. Ruangpornvisuti, B. Wanno, Physica E: Low-dimensional Systems
    and Nanostructures **49**, 61 (2013).
[13] S. Yang, W. Shin, J. Kang, Small **4**, 437 (2008).
[14] H. Bai, N. Yuan, Y. Wu, J. Li and Y. Ji, Fullerenes, Nanotubes and Carbon Nanostructures
    23, 203 (2015).
[15] Z. Xu, W. Lu, Adv. Mater. **20**, 3615 (2008).
[16] A. Du, Y. Chen, J. Am. Chem. Soc. **131**, 1682 (2009).
[17] E. Cruz-Silva, F. Lopez-Uras, ACS Nano **3**, 1913 (2009).
[18] M. R. Zardoosta, B. Dehbandib, Physica E: Low-dimensional Systems and Nanostructures

54, 226 (2013).

[19] P. A. Gowri sankar and K. Udhayakumar, J. Nanomater. **2013**, 293936 (2013).

[20] R. J. Baierle, S. B. Fagan, R. Mota, Antnio J. R. da Silva, and A. Fazzio, Phys. Rev. B **64**, 085413 (2001).

[21] R. Bian, J. Zhao, H. Fu, J. Mol. Model. **19**, 1667 (2013).

[22] S. B. Fagan, R. Mota, Antnio J. R. da Silva, and A. Fazzio, Nano Lett. **4**, 975 (2004).

[23] S. B. Fagan, R. Mota, R. J. Baierle, Antnio J.R. da Silva, A. Fazzio, Mater. Characterization **50**, 183 (2003).

[24] R. Lortza, Q. Zhang, W. Shi, J. T. Ye, C. Qiu, Z. Wang, H. He, P. Sheng, T. Qian, Z. Tang, N. Wang, X. Zhang, J. Wang and C. T. Chan, PNAS **106**, 7299 (2009).

[25] G. Chen, Y. Seki, H. Kimura, S. Sakurai, M. Yumura, K. Hata, D.N. Futaba, Scientific Reports **4**, 3804 (2014).

[26] Z. Zhou, M. Steigerwald, M. Hybertsen, L. Brus and R.A. Friesner, J. Amer. Chem. Soc. **126**, 3597 (2004).

[27] M. J. Frisch, G. W. Trucks, H. B. Schlegel, G. E. Scuseria, M. A. Robb and et al., Gaussian 09, Gaussian, Inc., Wallingford CT, (2009).

[28] H. Bai, W. Ji, X. Liu, L. Wang, N. Yuan and Y. Ji, Journal of Chemistry, **2013**, 571709 (2013).

[29] H.W. Wang, B.C. Wang, W.H. Chen and M. Hayashi, J. Phys. Chem. A **112**, 1783 (2008).

[30] R. C. Haddon and L. T. Scott, Pure App. Chem. **58**, 137 (1986).

[31] H. Bai, Y. Zhu, N. Yuan, Y. Ji, W. Qiao and Y. Huang, Chinese J. Struct. Chem. **32**, 695 (2013).

[32] V. Barone, O. Hod, G. E. Scuseria, Nano Lett. **6**, 2748 (2006).

[33] H. Bai, Y. Zhu, W. Qiao and Y. Huang, RSC Adv. **1**, 768 (2011).

[34] L.V. Liu, W.Q. Tian, Y.K. Chen, Y.A. Zhang, Y.A. Wang, Nanoscale **2**, 254 (2010).

[35] P. R. Schleyer, C. Maerker, A. Dransfeld, H. Jiao, N. J. R. E.Hommes, J. Am. Chem. Soc. **118**, 6317 (1996).

[36] H. Fallah-Bagher-Shaidaei, C. S. Wannere, C.. Corminboeuf, R. Puchta, P. v. R. Schleyer, Org. Lett. **8**, 863 (2006).

[37] L. V. Liu, W. Q. Tian, Y. K. Chen, Y. A. Zhang, Y. A. Wang, Nanoscale **2**, 254 (2010).

[38] J. Zhao and P. B. Balbuena, J. Phys. Chem. C **112**, 3482 (2008).

[39] M. Aghamohammadi , P. Shahdousti, R. Ghafouri, M. Anafcheh, Superlattice Microstruct. **57**, 66 (2013).

[40] R. Ghafouri, M. Anafcheh, Superlattice Microstruct. **55**, 33 (2013).

[41] Y. Ouyang, J. Peng, H. Wang and Z. Peng, Chinese Phys. B **17**, 3123 (2008).

[42] M. Z. Chen, R. B. King, Chem. Rev. **105**, 3613 (2005).